

Soft metal constructs for large strain sensor membrane

This content has been downloaded from IOPscience. Please scroll down to see the full text.

View [the table of contents for this issue](#), or go to the [journal homepage](#) for more

Download details:

IP Address: 128.179.180.238

This content was downloaded on 11/02/2015 at 08:13

Please note that [terms and conditions apply](#).

Soft metal constructs for large strain sensor membrane

Hadrien O Michaud, Joan Teixidor and Stéphanie P Lacour

École Polytechnique Fédérale de Lausanne (EPFL), Center for Neuroprosthetics, STI — IMT/IBI — LSBI, CH-1015 Lausanne, Switzerland

E-mail: stephanie.lacour@epfl.ch

Received 26 August 2014, revised 3 December 2014

Accepted for publication 16 December 2014


Published 10 February 2015



CrossMark

Abstract

Thin gold films on silicone display large reversible change in electrical resistance upon stretching. Eutectic liquid metal conductors maintain bulk metal conductivity, even upon extensive elongation. When integrated together, the soft metals enable multidirectional, large strain sensor skin. Their fabrication process combines thermal evaporation of thin gold film patterns through stencil mask with microplotting of eutectic gallium indium microwires, and packaging in silicone rubber. Using three-element rectangular rosettes, we demonstrate a sensor skin that can reliably and locally quantify the plane strain vector in surfaces subject to stretch (up to 50% strain) and indentation. This hybrid technology will find applications in soft robotics, prosthetics and wearable health monitoring systems.

 Online supplementary data available from stacks.iop.org/sms/24/035020/mmedia

Keywords: soft conductors, additive manufacturing, large strain sensing, miniaturized strain rosette

(Some figures may appear in colour only in the online journal)

1. Introduction

Strain sensors are implemented in nearly all fields of engineering, from infrastructure and automotive structural health monitoring [1, 2] to implantable bioelectronic systems [3]. Typical metal-foil strain gauges monitor small deformations, reported in microstrain. Systems including soft robots [4], data gloves [5, 6], skin-like electronics [7] and implantable bioelectronics [8] require distributed and high-strain sensing capabilities, which are unmet with today's technology. The recent translation of micro/nanofabrication techniques to soft, mechanically compliant carrier substrates provides an opportunity for new strain-sensing devices calibrated for large deformation, high sensitivity and conformal wearability [9].

The development of large strain sensitive devices involves designs with reversibly stretchable, electrically conductive materials and decoupling of the electro-mechanical response of the lead wires from that of the sensing element [10–12]. Stretchable conductors can be prepared with thin films on silicone, [13–16] elastomeric composites, [17–19] self-similar serpentine [20, 21] or liquid metals [22–24].

Thin gold films on PDMS are highly stretchable (to tens of percent over millions of cycles) [25] and display large relative change in their electrical resistance with applied elongation. Liquid metal conductors are also extremely elastic (with reported maximal stretchability to 600% strain [26]) and maintain very stable electrical conductivity even upon large deformation. In this work, we combine the benefits of both soft metallization techniques to fabricate compact strain gauges sensitive to large deformation and patternable over large area surfaces. The sensors and interconnects are embedded in silicone (PDMS, Dow Corning Sylgard 184). The proposed process is compatible with planar and additive manufacturing techniques thereby enables fully elastic inter-connected sensors and efficient decoupling of the strain responses in the wiring and sensing elements.

Stretchable gauges are defined by patterning stretchable thin gold films [13] with high absolute resistance $R_{0,Au}$ at zero strain, and high relative and absolute increase in resistance under large strains. They are connected with stretchable wires made of the eutectic alloy of gallium and indium (EGaIn, 75% Ga, 25% In in weight), with low absolute resistance

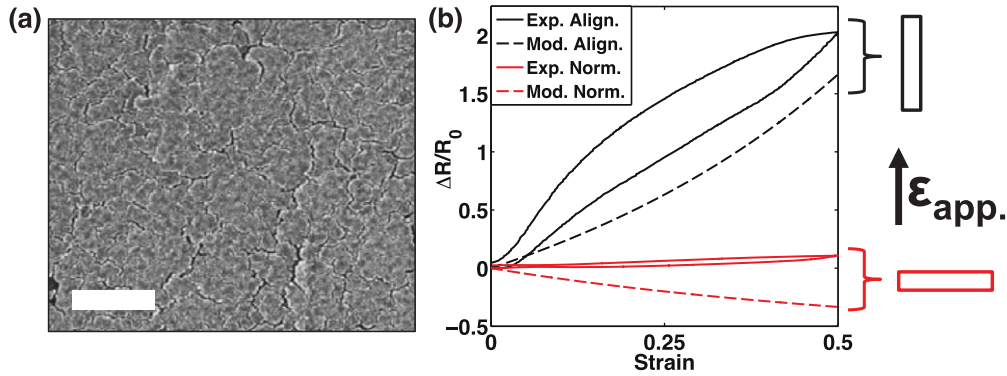


Figure 1. (a) SEM image of 25 nm thin micro-cracked Au film on PDMS. Scale bar is 1 μm . (b) Change in resistance of a strain gauge made of a $5 \times 0.5 \text{ mm}^2$ micro-cracked gold track on PDMS substrate when applying aligned and normal strain. Comparison between experimental measurements performed on 25 nm Au thin films on PDMS (solid lines) and output of model (dotted lines). Initial resistance R_0 is 138 Ω for the aligned (black) gauge and 131 Ω for the normal (red) gauge.

$R_{0,\text{EGaIn}}$ at zero strain, and low relative and absolute increase in resistance under strain [27]. For patterning the interconnects, we developed a technique similar to the one reported in [28] in order to plot two-dimensional continuous patterns of EGaIn. This method is additive and does not involve any masking process nor specific surface treatment. Hence, the wiring scheme can be easily and ‘instantly’ adapted to a new layout. In addition, our approach does not require complex design rules nor substrate preparation such as pre-strain since the metallic conductors used here are intrinsically stretchable. We apply this process to fabricate integrated sensing devices featuring up to three localized strain sensitive areas within less than 30 mm^2 . By adapting the classical theoretical framework for strain gauges, we are able to quantify the amplitude and orientation of large ($>10\%$) strains, and discriminate uniaxial from multiaxial deformation of the soft substrate.

2. Results

2.1. Stretchable gold film patterns as directional large strain sensors

100 mm silicon wafers were coated with a self-assembled layer of trichloro(1 H,1 H,2 H,2 H-perfluorooctyl)silane from Sigma Aldrich to ease release of structures after integration. Sylgard 184 base and curing agent from Dow Corning were mixed in a 10:1 ratio (Thinky ARE-250) and degassed under vacuum. Then, the uncured PDMS was spin-coated at 500 RPM for 1 min in order to form an approximately $120 \mu\text{m}$ thick layer. Coated wafers were placed in an oven (VWR Venti-Line) for 2 hours at 80°C to cure the PDMS layer. Bilayers of Cr (5 nm) and Au (25 to 40 nm) were thermally evaporated on the PDMS substrate. Polyimide shadow masks were mounted directly on the PDMS substrate to define patterns of metallic conductor.

Figure 1(a) displays a scanning electron microscope image of a thin gold film thermally evaporated on a PDMS

substrate. The typical sheet resistance of the 25 nm thick metal on PDMS is around $20 \Omega/\text{sq}$, more than 10 times that of a similar Au film deposited on a hard carrier [29]. Figure 1(b) describes the relative change in resistance $\Delta R/R_0$ of a $5 \times 0.5 \text{ mm}^2$ gold thin film track on PDMS during uniaxial stretch cycle to 50% applied strain ϵ_{app} . Significant resistance increase is observed when the Au line is aligned with the strain direction ($\Delta R/R_0 = 2$ at $\epsilon_{\text{app}} = 0.5$) while nearly no change can be recorded when the film is stretched transversely ($\Delta R/R_0 \approx 0$ at $\epsilon_{\text{app}} = 0.5$). Their typical gauge factor is about 4, in agreement with reported values of $20 \Omega/\text{sq}$ for very thin metal films subject to microstrain deformation [30].

Gold films evaporated on PDMS with thickness in the 20–100 nm range form a nearly discontinuous network of gold ligaments (figure 1(a)). Such microstructure is typical of thin ($<100 \text{ nm}$ thick) metal films deposited by evaporation, [30–32] and results from interplay between the granular growth of evaporated metal films and the large thermal expansion coefficient of the underlying PDMS substrate ($\text{CTE}_{\text{PDMS}} = 300 \text{ ppm}/^\circ\text{C}$). The built-in microcracks in the thin Au film on PDMS allow for the microscopic gold bands to bend and twist locally out of the plane thereby accommodating (in a reversible manner) large, macroscopic, applied deformation of the substrate [33]. The film retains its microstructure upon stretching to high strain and over many cycles, and maintains stable electrical conduction [25]. Electrically, the film is more resistive than a bulk, uniform film of similar thickness, and its relative change in resistance with applied strain is larger than that due to pure geometrical rearrangement.

Let’s consider an elastic and uniform conductor of $L \times W \times T$ (length \times width \times thickness) geometry. Assuming its electrical resistivity remains constant upon stretching, $\Delta R/R_0$ depends on the relative change in the geometric factor $L/(WT)$, and can be expressed as a function of the applied strain ϵ_{app} and is plotted figure 1(b).

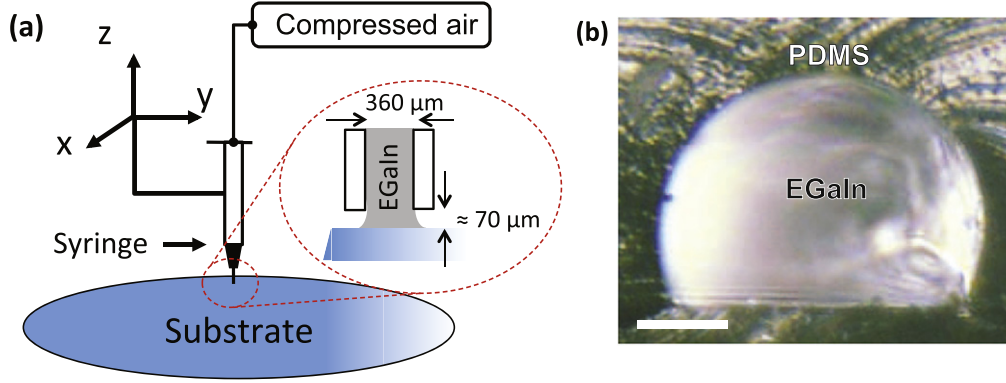


Figure 2. (a) Schematic of the EGaln microwires plotting set-up. (b) Cross section of a liquid metal wire encapsulated in PDMS. Scale bar is 50 μm .

When the length of the conductor is aligned with the direction of ϵ_{app}

$$\left(\frac{\Delta R}{R_0}\right)_{\text{align.}} = \frac{1 + \epsilon_{\text{app}}}{(1 - \nu\epsilon_{\text{app}})^2} - 1. \quad (1)$$

When the length of length of the conductor is normal to the direction of ϵ_{app}

$$\left(\frac{\Delta R}{R_0}\right)_{\text{norm.}} = \frac{(1 - \nu\epsilon_{\text{app}})}{(1 + \epsilon_{\text{app}})(1 - \nu\epsilon_{\text{app}})} - 1, \quad (2)$$

where ν is the substrate's Poisson ratio.

We observe that the experimental $\Delta R/R_0$ is much larger than that of a plain conductor ongoing pure elastic deformation for both aligned and normal strain (figure 1(b)). This divergence might be explained by the evolution of the film structure [25] and the conduction mechanism within the gold ligaments (percolation) and across the microcracks (tunneling) with applied strain. Those phenomena can be modeled with the help of empirical observations [34].

The gauge factor $GF = \Delta R/(R_0\epsilon_{\text{app}})$ of a gold track varies over a stretching cycle, due to nonlinearity and hysteresis. We define the average gauge factor \overline{GF} as $\overline{GF} = \Delta R/(R_0\epsilon_{\text{app,max}})$, where $\epsilon_{\text{app,max}} > 0$ is the maximum applied tensile strain along the long axis of the gauge. As reported for gold thin films under microstrain [30], there seems to be a correlation between the initial sheet resistance of the thin films and their gauge factor (see figure S1). The average gauge factor remains stable before and after encapsulation with a thick layer of PDMS.

Patterns of stretchable thin metal film on PDMS gather the required properties to be used as large strain gauges.

2.2. EGaln microwires for stretchable interconnects

Microstructures of liquid metals can be plotted, printed or micromolded on the surface of PDMS [22, 35, 36]. We have developed a micro-plotting technique similar to that reported by Boley *et al* [28]; its schematic is highlighted figure 2(a). Fast and direct writing of microwires of EGaln is performed by dispensing in a continuous flow small amount of EGaln

(99.99%, Sigma Aldrich), preliminarily loaded in a syringe mounted on a computer-controlled three-axis XYZ micro-positioner stage (Sonoplot GX-II Microplotter). The soft metal wires are plotted directly on a PDMS membrane spun and cured on silicon carrier wafer. The inner diameter of the syringe tip was 360 μm . The pressure inside the syringe reservoir was maintained in the 1–5 kPa range using a fluid dispenser (OK International TS250) to force the liquid to reach the end of the syringe's tip without forming a droplet. The tip was put in contact with the substrate and then slightly raised vertically (20 to 80 μm above the substrate) in order to form a liquid metal meniscus. Next, the tip was moved in the horizontal plane at 200 $\mu\text{m s}^{-1}$, allowing the liquid metal to flow on the substrate and form wires. Silver wires were put into contact with the terminals of the liquid metal wires and a small drop of curable silver paste or EGaln was put on top of the contact point to enhance the electrical connection. The contact area was subsequently encapsulated using silicone sealant (Dow Corning 732). Thanks to the good adhesion between the oxide skin that forms around the wires and the PDMS substrate, patterns composed of microwires were encapsulated by spin-coating uncured PDMS at 250 RPM. Finally, the encapsulation layer was cured at 60 $^{\circ}\text{C}$ for 12 hours and the devices were cut and peeled off the support wafer. The total thickness of the integrated devices was below 500 μm . Figure 2(b) displays a cross-sectional view of an encapsulated soft conductor.

We performed '4-wire' resistance measurements on soft microwires on PDMS substrate without encapsulation. A Keithley 2400 sourcemeter was used in preconfigured 4-wire remote sensing mode, with automatic current selection, in the 20 Ω range with 100 $\mu\Omega$ resolution. In this range, the accuracy of the measurement was given by $\Delta R = 0.010\% \times R_{\text{measured}} + 3 \text{ m}\Omega$ according to the instrument's manual [37]. Due to the small size of the lines (about 5 mm long and 150 μm wide) four hook probes mounted on XYZ positioners were used to precisely contact the EGaln line. Each probe held a 76 μm diameter Au wire (science products) which was put in contact with the liquid metal wire. The two outer probes were positioned at the two opposite ends of the wire. The distance L_w between the two inner probes (see figure S3), which defined the 4-wire resistance, was measured

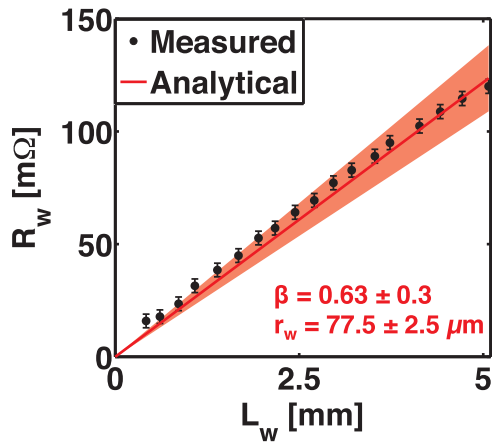


Figure 3. Comparison between 4-wire resistance measurement and resistance computed from equation (3). Error bars represent measurement accuracy. Shaded area represent 95% confidence interval for the output values of the analytical model.

with a digital microscope (Keyence VHX-600, VH-Z50L lens). As the hard probing wires may have damaged the liquid metal wire in the vicinity of the contact point, the spacing between the two inner probes was first set to a maximum of 5 mm and then sequentially reduced to collect the data points. The measured resistances for various wire lengths are compared with the output of an analytical model and shown in figure 3. The EGaln microwire is modeled as a metallic semi-cylinder with a constant resistivity $\rho = 29.4 \times 10^{-6} \Omega\text{cm}$ [38] and a truncated circular cross-section with radius r_w . The corresponding resistance R_w is computed from the measured geometry of the wire using

$$R_w = \rho \frac{L_w}{\beta \pi r_w^2}, \quad (3)$$

where $\beta = 0.63 \pm 0.3$. r_w and β were experimentally determined after encapsulation by measuring the cross-section of the imprint left by the wire in the PDMS (figure 2(b)). The good agreement between the output of the model and the 4-wire resistance demonstrates the deposition process does not increase the resistivity of the liquid metal structures. It also suggests the encapsulation process does not impact the structure of the microwires. The average cross-section geometry corresponds to a contact angle of about 102° (see figure S2) at the interface between EGaln microwires and PDMS substrate. It is consistent with previously reported values for microwires with similar dimensions [28].

The EGaln microwires were stretched using a home-built, computer controlled, motorized uniaxial stretcher. Each end of the samples, including the contact area with silver wires, was clamped on a moving platform. Four-point electrical resistance and applied mechanical strain were recorded simultaneously at a frequency of 8 Hz. Figure 4 presents the electro-mechanical characterization of an EGaln microwire. The encapsulated liquid metal interconnects exhibit low absolute resistance at zero strain and low relative and absolute increase in resistance compared to stretchable gold thin films ($\Delta R_w \ll \Delta R_{\text{gauge}}$). Assuming the EGaln is incompressible, the

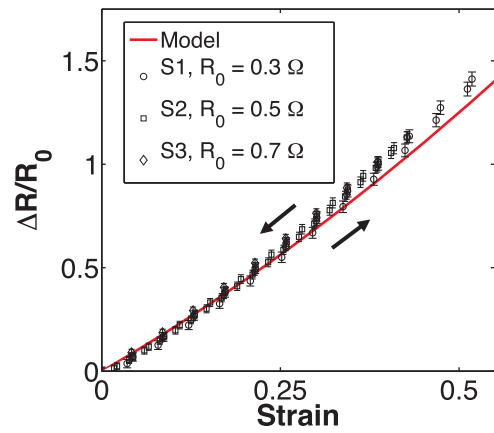


Figure 4. Electro-mechanical characterization of long EGaln wires encapsulated in PDMS under uniaxial strain and comparison with the constant volume model. Resistance was measured using four-point measurement method. Initial length of the wires was 25 mm (S1 and S3) and 30 mm (S2). Sample S1 was strained up to 50%, samples S2 and S3 up to 42%. Error bars represent measurement accuracy.

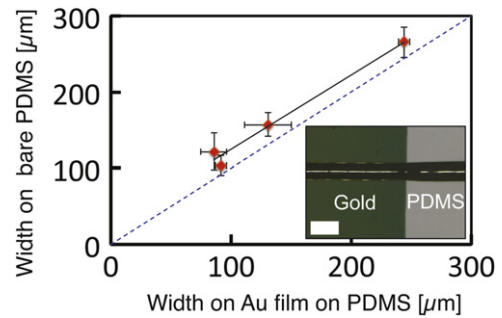


Figure 5. Continuous printing of EGaln wires on bare PDMS and PDMS coated with micro-cracked Au. Solid line represents least square linear fit and dashed line represents identity. Error bars represent 95% confidence interval. Line width was modulated by changing the syringe's height. Inset: line patterned on micro-cracked gold and bare PDMS. Scale bar is $150 \mu\text{m}$.

volume of the wires remains constant under elastic deformation and their relative increase in resistance as a function of applied mechanical strain ϵ_{app} can be expressed as

$$\frac{\Delta R}{R_0} = \left(\frac{L}{L_0} \right)^2 - 1 = \epsilon_{\text{app}} (2 + \epsilon_{\text{app}}). \quad (4)$$

Good correspondence between the model and experimental measurements (figure 4) indicates that no leakage occurred when the wires were stretched. Although soft EGaln microstructures can be used as strain sensitive elements [39], the direct patterning of the EGaln microwires and their minimal increase in resistance under mechanical deformation offer ideal characteristics for elastic interconnects.

2.3. Integrated strain gauges

PDMS substrates with patterns of micro-cracked gold were processed in the liquid metal dispensing set-up. EGaln microwires could be drawn continuously from the bare PDMS

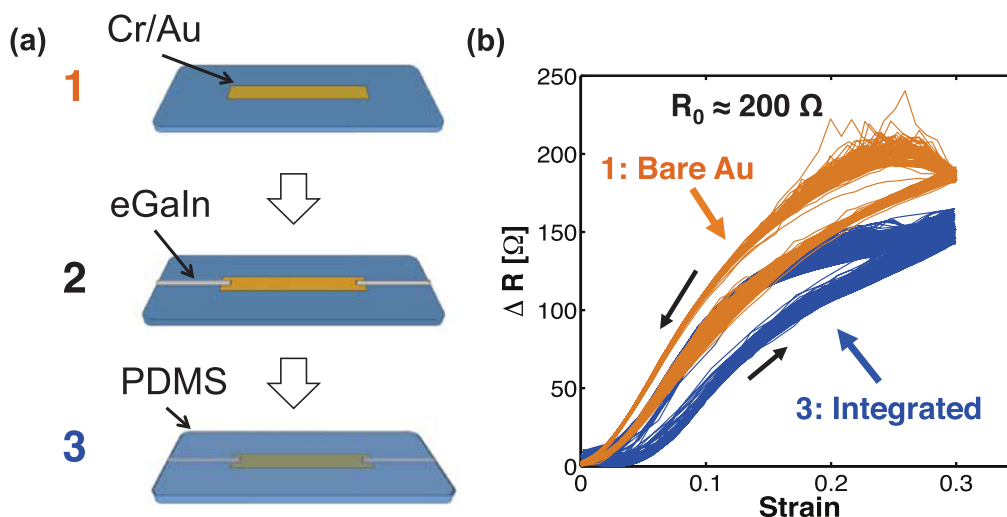


Figure 6. (a) Process flow for the fabrication of an integrated strain gauge made of micro-cracked gold and connected with EGaln microwires. (b) Comparison of the response of a non-encapsulated gold track probed with solid wiring, connected with silver filled epoxy adhesive (Epotek H27-D), and an integrated strain gauge with EGaln interconnects. 125 cycles are represented on this graph for each gauge. Length L and width W are 6 mm and 500 μm respectively.

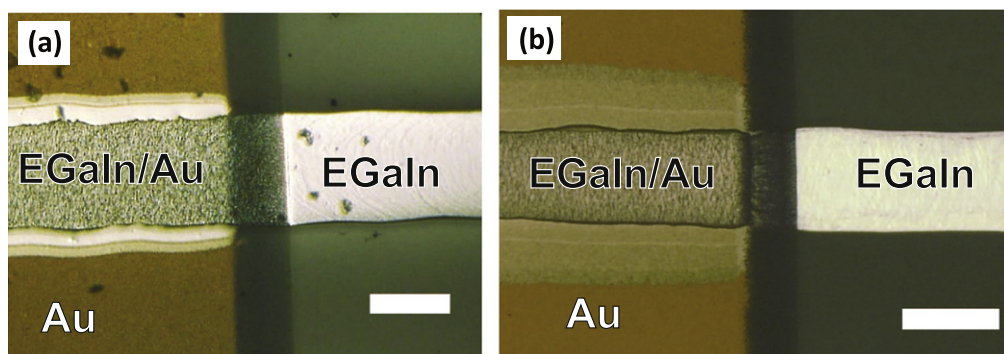


Figure 7. (a) Backside view of the contact zone between EGaln microwire and Au thin film on PDMS one week after integration. Scale bar is 200 μm . (b) Backside view of the contact zone between EGaln microwire and Au thin film on PDMS six months after integration. Scale bar is 200 μm .

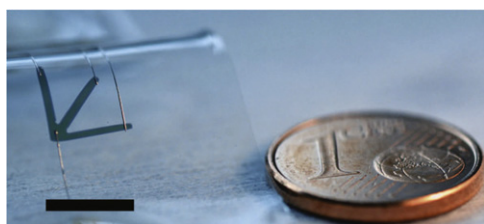


Figure 8. Picture of a rosette made of stretchable gold thin film connected with EGaln wires. Scale bar is 5 mm.

to the gold-coated areas and vice versa. We observed the EGaln microwires are slightly narrower on the PDMS coated with a stretchable gold film than on the bare PDMS (figure 5). This may be because the oxide skin of the liquid metal has more affinity with bare PDMS than with a micro-structured film [40]. Figure 6(a) presents the microfabrication process developed to integrate compact strain gauges with high and localized sensitivity. First a gold layer is thermally evaporated through a shadow mask on the PDMS substrate. Then, EGaln

interconnects are plotted using the direct writing system. The interconnected sensors are then encapsulated with a layer of PDMS.

Integrated single strain gauges were characterized in the customized stretcher. The strain rate was fixed between 1.25 and 1% s^{-1} when the number of strain cycles was below 100 and fixed to 5% s^{-1} for larger number of cycles. Prior to single gauge or rosette characterization measurements, about 50 cycles up to 50% strain were applied to the structures in order to reach a stable regime for the electro-mechanical response of Au tracks [25]. Figure 6(b) presents the electro-mechanical response of an integrated gauge with liquid metal interconnects at both ends, compared to the response of a non-encapsulated gold track with similar dimensions but probed with solid wiring. In the case of solid wire probes, silver-filled adhesive (Epotek H27-D) was used to maintain electrical contact between the wires and the soft gold films. Both samples are cycled up to 30% applied strain. No significant difference is observed between the response of the integrated strain gauges and the bare gold tracks when a large number of

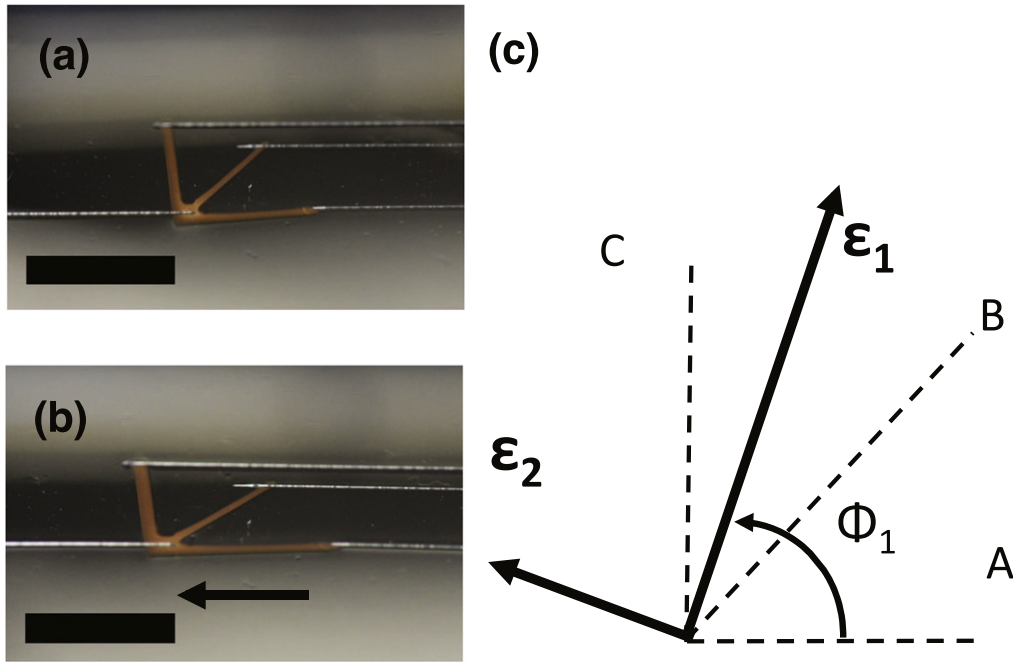


Figure 9. Rosette under (a) 0% uniaxial strain and (b) 50% uniaxial strain. Scale bars are 5 mm. (c) Orientation of the two principal strains relative to the three branches of the rosette.

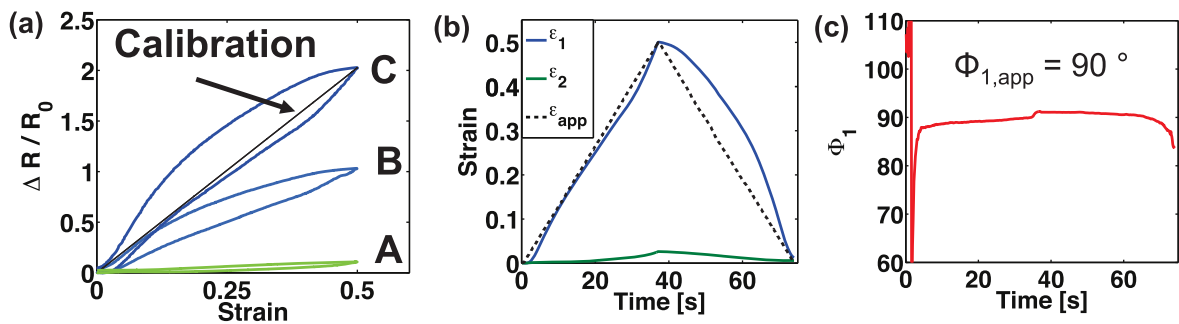


Figure 10. (a) Relative increase in resistance of branches A, B and C. (b) Computed magnitude of principal strains. (c) Computed orientation of the first principal strain, for a 50% maximal applied strain with an angle $\Phi_{1,app} = 90^\circ$ relative to branch A.

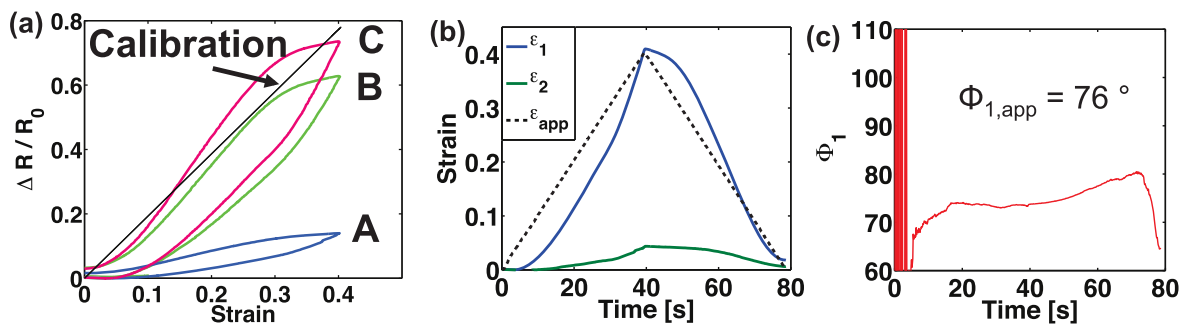


Figure 11. (a) Relative increase in resistance of branches A, B and C. (b) Computed magnitude of principal strains. (c) Computed orientation of the first principal strain, for a 40% maximal strain applied with an angle $\Phi_{1,app} = 76^\circ$ relative to branch A.

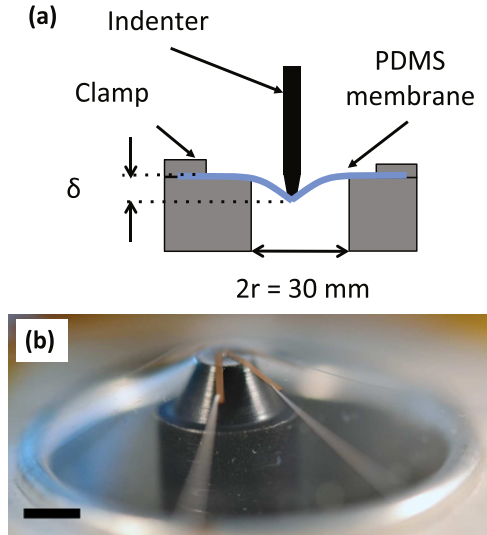


Figure 12. (a) Schematic of the experimental set-up used for inducing isotropic strain in the rosette. (b) Deformation of a PDMS membrane with integrated strain rosette during indentation. Scale bar is 5 mm.

strain cycles is applied. The strain sensitivity of the interconnects does not alter the thin Au film gauges' response to strain. The lower increase in resistance of the integrated strain gauge may be explained by the presence of the encapsulation layer and by the dispersion in gold tracks electrical characteristics due to the random nature of the microcracks (figure 1(a)). Furthermore, the absolute change in resistance of the soft gauges is more than two orders of magnitude higher than that of the liquid metal interconnects.

EGaIn alloys with gold, forming a compound 100 times more resistive than bulk gold [41]. If this alloy sits underneath EGaIn, it is electrically shorted by the liquid metal. However, as shown figure 7 the alloy appears to have diffused a few hundreds of microns around the contact point after six months storage in ambient conditions, resulting in a mean increase in base resistance of 42% (from $92 \pm 4\Omega$ to $131 \pm 7\Omega$ for 5×0.5 mm tracks). This effect does not seem to compromise the electro-mechanical behavior of the fabricated devices under strain (figure S4).

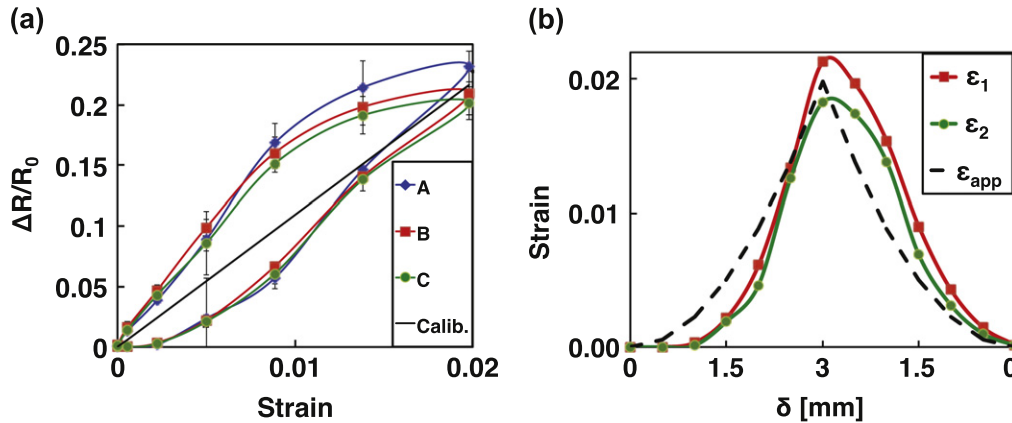


Figure 13. (a) Relative increase in resistance of gauge A, B and C as a function of approximated applied mechanical strain. Errors bars represent 95% confidence interval. (b) Magnitude of principal strains computed from the sensors' outputs as a function of indentation depth δ .

2.4. Compact rosettes for sensing strain magnitude and direction

Orientation and magnitude of uniaxial applied strain can be determined using three strain gauges arranged in a rectangular rosette configuration (figures 8 and 9). One of the three sensors, A–B–C, is first stretched along its long axis in order to determine the average gauge factor \overline{GF} of all three branches in the rosette. After this calibration step, the strain in each sensor A, B and C is determined using

$$\epsilon_{A,B,C} = \frac{1}{\overline{GF}} \left(\frac{\Delta R}{R_0} \right)_{A,B,C}. \quad (5)$$

In the rectangular rosette configuration, the principal strains $\epsilon_{1,2}$ and their orientation θ can be derived from the strains sensed by gauges A, B and C [42]

$$\epsilon_{1,2} = \frac{\epsilon_A + \epsilon_C}{2} \pm \frac{1}{\sqrt{2}} \sqrt{(\epsilon_A - \epsilon_B)^2 + (\epsilon_C - \epsilon_B)^2}, \quad (6)$$

$$\theta = \frac{1}{2} \tan^{-1} \left(\frac{\epsilon_A - 2\epsilon_B + \epsilon_C}{\epsilon_A - \epsilon_B} \right). \quad (7)$$

The angle Φ_1 , between direction A and ϵ_1 , is determined from θ by comparing between ϵ_A , ϵ_B and ϵ_C (see supporting information) [43].

Figures 10 and 11 present the outputs of the strain gauge rosette. ϵ_2 is not null but remains smaller than $\epsilon_1/10$ thanks to the small transverse sensitivity of the gauges. When the applied strain is aligned with one of the sensors, the computed angle clearly matches one of the gauge direction (figure 10(c)). Arbitrary strain orientation is also nicely detected (figure 11(c)).

The soft metal sensor skin can also reliably monitor isotropic strains. A PDMS circular membrane (about 50 mm in diameter) with a strain rosette integrated at its center was attached on top of a mechanical support with a 30 mm diameter hole at its center. The three gold tracks composing the rosette were oriented radially from the center of the membrane. The common contact of the rosette was aligned with the center of the hole and the tip of an indenter. A load frame (MTS Systems Criterion C42.503) was used to control the

indentation depth. A small piece of PDMS (1 mm in diameter, 1 mm in thickness) was put between the hard indenter and the soft membrane in order to minimize undesired local stress concentration at the center of the membrane. A schematic is also displayed figures 12(a) and (b) shows the freestanding circular PDMS membrane with a rosette integrated at its center indented using a load frame. An approximation of the strain induced in the membrane is calculated from

$$\epsilon_{\text{app}} = \sqrt{1 + \left(\frac{\delta}{r_m}\right)^2} - 1, \quad (8)$$

where $r_m = 15$ mm is the radius of the circular membrane, and δ is the indentation depth (between 0 and 3 mm). We do not take into account nonlinearity in the membrane profile [44], nor local microscopic strain concentration at the edge of the tip. The relative increase in resistance in the three branches of the rosette are almost identical (figure 13(a)), thus the magnitude of the two principal strains ϵ_1 and ϵ_2 are similar (figure 13(b)). In this situation, Φ_1 remains indeterminate since $\epsilon_A \simeq \epsilon_B \simeq \epsilon_C$ [43].

3. Conclusion

In summary, we demonstrate a novel combination of stretchable gold thin films and liquid metal microwires to produce soft metal electronic skins. Stretchable gold thin films deposited on soft PDMS substrate define conductive rectangular sensors that are highly sensitive to tensile strains. Once interconnected with highly conductive and stretchable liquid metal microwires, the soft sensors can be integrated on large-area patterns. This additive integration method enables fast and easy redistribution of the interconnects when the layout of the sensors is changed. Compact strain sensors with thickness under 0.5 mm stretch reliably up to 50%. Even larger deformation may be possible if needed.

The integration process of the soft strain gauges does not alter the electro-mechanical response of gold thin films nor the conductivity of the EGaIn wires. By arranging the strain sensors in rectangular rosettes and applying classical strain gauge theory, we were able to measure the strain vector (magnitude and direction of uniaxial strain) and discriminate between uniaxial and isotropic strain fields. Future work will involve improving on the integration and sensor's density by, for example, developing vertical, via-like connections between stacked layers of sensors, and coupling strain sensitive structures to other transducers. Integrated mechano-sensitive electronic skins will find application in smart textiles, robotics and rehabilitation prosthetics.

Acknowledgments

This work was funded by the Nano-tera.ch initiative (20NA21 143070 WiseSkin).

References

- [1] Farrar C R and Worden K 2007 *Phil. Trans. R. Soc. A* **365** 303–15
- [2] Ko J and Ni Y 2005 *Eng. Struct.* **27** 1715–25
- [3] Burr D B, Milgrom C, Fyhrie D, Forwood M, Nyska M, Finestone A, Hoshaw S, Saiaj E and Simkin A 1996 *Bone* **18** 405–10
- [4] Pfeifer R, Lungarella M and Iida F 2012 *Commun. ACM* **55** 76–87
- [5] Borghetti M, Sardini E and Serpelloni M 2013 *IEEE Trans. Instrum. Meas.* **62** 3308–14
- [6] Yan C, Wang J, Kang W, Cui M, Wang X, Foo C Y, Chee K J and Lee P S 2013 *Adv. Mater.* **26** 2022–7
- [7] Hammock M L, Chortos A, Tee B C K, Tok J B H and Bao Z 2013 *Adv. Mater.* **25** 5997–6038
- [8] Kim D H *et al* 2012 *Proc. Natl Acad. Sci. USA* **109** 19910
- [9] Park Y L, Chen B R, Pérez-Arancibia N O, Young D, Stirling L, Wood R J, Goldfield E C and Nagpal R 2014 *Bioinsp. Biomimetics* **9** 016007
- [10] Lu N, Lu C, Yang S and Rogers J 2012 *Adv. Funct. Mater.* **22** 4044–50
- [11] Ying M, Bonifas A P, Lu N, Su Y, Li R, Cheng H, Ameen A, Huang Y and Rogers J A 2012 *Nanotechnology* **23** 344004
- [12] Chossat J B, Park Y L, Wood R J and Duchaine V 2013 *IEEE Sensors J.* **13** 3405–14
- [13] Lacour S P, Wagner S, Huang Z and Suo Z 2003 *Appl. Phys. Lett.* **82** 2404
- [14] Wagner S, Lacour S P, Jones J, Hsu P I, Sturm J C, Li T and Suo Z 2004 *Physica E* **25** 326–34
- [15] Vijay V, Rao A D and Narayan K S 2011 *J. Appl. Phys.* **109** 084525
- [16] Yu C, Wang Z, Yu H and Jiang H 2009 *Appl. Phys. Lett.* **95** 141912
- [17] Sekitani T, Noguchi Y, Hata K, Fukushima T, Aida T and Someya T 2008 *Science* **321** 1468–72
- [18] Rosset S, Niklaus M, Dubois P and Shea H R 2009 *Adv. Funct. Mater.* **19** 470–8
- [19] Xu F and Zhu Y 2012 *Adv. Mater.* **24** 5117–22
- [20] Gonzalez M, Axisa F, Bulcke M V, Brosteaux D, Vandeveldel B and Vanfleteren J 2008 *Microelectron. Reliab.* **48** 825–32
- [21] Fan J A *et al* 2014 *Nat. Commun.* **5** 3266
- [22] Dickey M D, Chiechi R C, Larsen R J, Weiss E A, Weitz D A and Whitesides G M 2008 *Adv. Funct. Mater.* **18** 1097–104
- [23] Cheng S, Rydberg A, Hjort K and Wu Z 2009 *Appl. Phys. Lett.* **94** 144103
- [24] Wagner S and Bauer S 2012 *MRS Bull.* **37** 207–13
- [25] Graz I M, Cotton D P J and Lacour S P 2009 *Appl. Phys. Lett.* **94** 071902
- [26] Zhu S, So J H, Mays R, Desai S, Barnes W R, Pourdeyhimi B and Dickey M D 2013 *Adv. Funct. Mater.* **23** 2308–14
- [27] Kim H, Maleki T, Wei P and Ziaie B 2009 *J. Microelectromech. Syst.* **18** 138–46
- [28] Boley J W, White E L, Chiu G T C and Kramer R K 2014 *Adv. Funct. Mater.* 3501–7
- [29] Wissmann P 2007 *Electrical Resistivity of Thin Metal Films* (Berlin: Springer)
- [30] Neuman M R 1969 *J. Vac. Sci. Technol.* **6** 710
- [31] Meiksin Z H 1967 *J. Appl. Phys.* **38** 4490
- [32] Parker R L and Krinsky A 1963 *J. Appl. Phys.* **34** 2700
- [33] Lacour S P, Chan D, Wagner S, Li T and Suo Z 2006 *Appl. Phys. Lett.* **88** 204103
- [34] Cao W, Gorn P and Wagner S 2011 *Appl. Phys. Lett.* **98** 212112
- [35] Kramer R K, Majidi C and Wood R J 2013 *Adv. Funct. Mater.* **23** 5292–6

- [36] Ladd C, So J H, Muth J and Dickey M D 2013 *Adv. Mater.* **25** 5081–5
- [37] Keithley Instruments Inc 2011 *Series 2400 SourceMeter Specifications*
- [38] Zrnic D and Swatik D 1969 *J. Less-Common Met.* **18** 67–68
- [39] Majidi C, Kramer R and Wood R J 2011 *Smart Mater. Struct.* **20** 105017
- [40] Kramer R K, Boley J W, Stone H A, Weaver J C and Wood R J 2014 *Langmuir* **30** 533–9
- [41] Kim H J 2007 Stretchable interconnects using room temperature liquid alloy on elastomeric substrate *PhD Thesis* Purdue University
- [42] Watson R B 2008 *Springer Handbook of Experimental Solid Mechanics* ed W N Sharpe Jr and W N Sharpe (Berlin: Springer) pp 283–333
- [43] Perry C 1989 *Exp. Tech.* **13** 13–18
- [44] Liu K and Ju B 2001 *J. Phys. D: Appl. Phys.* **91** 91–94